Pavel A. Perezhogin*

Testing of kinetic energy backscatter parameterizations in the NEMO ocean model

https://doi.org/10.1515/rnam-2020-0006
Received January 15, 2020; accepted January 16, 2020

Abstract: Eddy-permitting numerical ocean models resolve mesoscale turbulence only partly, that leads to underestimation of eddy kinetic energy (EKE). Mesoscale dynamics can be amplified by using kinetic energy backscatter (KEB) parameterizations returning energy from the unresolved scales. We consider two types of KEB: stochastic and negative viscosity ones. The tuning of their amplitudes is based on a local budget of kinetic energy, thus, they are 'energetically-consistent' KEBs. In this work, the KEB parameterizations are applied to the NEMO ocean model in Double-Gyre configuration with an eddy-permitting resolution (1/4 degree). To evaluate the results, we compare this model with an eddy-resolving one (1/9 degree). We show that the meridional overturning circulation (MOC), meridional heat flux, and sea surface temperature (SST) can be significantly improved with the KEBs. In addition, a better match has been found between the time power spectra of the eddy-permitting and the eddy-resolving model solutions.

Keywords: Two-dimensional turbulence, stochastic parameterization, kinetic energy backscatter, subgrid scale modeling, ocean dynamics, mesoscale eddies.

MSC 2010: 76F25, 76F65, 86A05, 60H30

Numerical ocean models used in climate research have a relatively coarse resolution to properly resolve mesoscale eddies, which contribute largely to the transport of scalars and momentum. Mesoscale eddies emerge on the length scale of the Rossby radius of deformation due to baroclinic instability, and in the mid-latitude ocean their qualitative length scale is 30 km. Considering the ability to resolve mesoscale eddies, the ocean general circulation models (OGCMs) can be divided into three groups: 'non-eddy-resolving' models have an approximate resolution of 1° and cannot simulate mesoscale eddies; 'eddy-resolving' models have several mesh points for a mesoscale eddy and their resolution is 10 times finer. Finally, there are models named 'eddy-permitting' which have an intermediate resolution. In the eddy-permitting models eddies are represented in a computational grid, but their dynamics and generation are damped. Currently, the OGCMs used in climate research (CMIP6) are changing from non-eddy-resolving to eddy-permitting resolutions [17].

Let us explain the difference between non-eddy-resolving and eddy-permitting models from the viewpoint of turbulence research. Non-eddy-resolving OGCMs can be considered as RANS (Reynolds-Averaged Navier-Stokes) simulations of quasi-2D turbulence, where the action of mesoscale turbulent motions is represented by the mean Reynolds stress. On the other hand, eddy-permitting OGCM is a Large eddy simulation (LES, [35]) of partly-resolved turbulent field. So, not only mean values of Reynolds stress, but also its time variations can be modelled to improve simulation, see [3] for more details. Turbulent viscosity model of Reynolds stress can be applied to both resolutions, but it has negative impact on LES simulations in the following meaning. Due to the smoothing action, large turbulent viscosity leads to increasing of simulated turbulence field in spatial scale and reduces effective resolution of LES simulation. So, the attractive research direction is to construct turbulent closures of quasi-2D turbulence for eddy-permitting OGCMs that overcome smoothing property of usual turbulent viscosity parameterization.

There are alternative parameterizations of subgrid eddies. Scale-similarity model (SSM, [2]) filters resolved turbulence field into small- and large-scale parts, followed by the computation of their interaction. Dynamic model [18] analyses SSM tendency and estimates energy flux towards unresolved scales in order to

***Corresponding author: Pavel A. Perezhogin,** Marchuk Institute of Numerical Mathematics of the Russian Academy of Sciences, Moscow 119333, Russia. E-mail: pperezhogin@gmail.com

adjust eddy viscosity coefficient. Concerning quasi-2D flows, these subgrid closures were studied only in the simplest barotropic models [5, 28, 30, 31]. We can guess why they were not applied to more complex quasi-2D models: in contrast to 3D turbulence (where they are popular), 2D one is characterized by the dual cascade of energy end enstrophy [22], as a result, SSM model captures both these fluxes (see Fig. 3 in [31]). Unfortunately, SSM model is inaccurate and cannot guarantee proper balance between energy and enstrophy fluxes. So, it is more attractive to simulate consequences of dual cascade by different turbulence closures: one for enstrophy flux towards subgrid scales (turbulent viscosity) and another one for energy flux from subgrid scales (Kinetic Energy Backscatter, KEB, [7]). Also we mention parameterizations designed specially for 2D turbulence: in [20] subgrid scales are simulated stochastically which gives subgrid force tendency, in [27] stochastic tendency corresponds to probability distribution conditioned on the observed flow and in [29] artificial neural network approach is considered.

KEB is a parameterization which returns energy from unresolved turbulent scales to resolved ones, contrary to eddy viscosity. This parameterization models poorly resolved inverse energy cascade inherent to 2D turbulence. Concerning quasi-2D flows, one of the first experiments with KEB was devoted to barotropic turbulence on a sphere [11]. Later, stochastic KEB was used to increase ensemble spread in weather prediction system [4]. Recently it was proposed to use KEB parameterizations to improve eddy-permitting ocean simulations [12, 13]. The simplest KEB closures are based on the Laplace operator with a negative viscosity coefficient [12, 13] (another linear operator is possible [15, 21, 36]) or on a stochastic tendency [12, 19]. KEB were shown to be effective in restoration of the barotropic eddy kinetic energy spectrum [12, 13, 31] and the mean flow [12, 13]. It improves barotropic instability simulation: KEB leads to reduction of error norms [21] and to increasing in increments of unstable modes [30]. In spite of the success in simulations with simplified quasi-geostrophic equations, long time experiments in GCMs appeared only recently: flow in reentrant channel [15], 'Neverworld' configuration in the MOM ocean model [14], global ocean configuration [16], and experiments with idealized models of atmosphere [8, 38]. These works show large improvements in reproducing of the first and second moments of the flow statistics.

In this work we apply two KEB parameterizations, negative viscosity and stochastic ones, to improve the NEMO ocean model [25, 26] at coarse eddy-permitting resolution (1/4°) in Double-Gyre configuration [24]. Intending to improve the mesoscale physics, we compare coarse models with respect to an eddy-resolving one (1/9°), which allows for mesoscales eddies, but not submesoscale ones. Both KEBs are introduced into momentum equations, and they are 'energetically consistent', which means that we tune the KEB amplitude to compensate the kinetic energy loss due to eddy viscosity. The prohibition of energy transfer to the subgrid scales is natural, since dynamics of 2D fluids redistributes energy into large scales in many configurations of the experiments (see [9, 32–34]). The possibility of returning not only kinetic, but also potential energy, is discussed in [3, 21, 37]. Here we follow the simplest approach. Similarly to [13] and [15], we define the negative viscosity KEB with coefficient depending on the amount of subgrid energy. The computation stability is ensured by biharmonic eddy viscosity damping. The stochastic KEB has the functional form of a random streamfunction weighted by the local dissipation rate, as proposed in [4]. The spatial correlation is controlled by multiple applications of a simple spatial filter to the generated spatial white noise, as proposed in [19]. Both KEB parameterizations increase the eddy kinetic energy (EKE) in an eddy-permitting model. It makes the meridional eddy heat flux close in eddy-permitting and eddy-resolving models. As a result, the sea surface temperature (SST) and the meridional overturning circulation (MOC) were restored with the use of KEB. Finally, we report improvements in the time power density spectrum.

1 Double Gyre setting

We use an open access NEMO model (version 3.6) [26] in Double-Gyre configuration described in [24]. Note that there is some discrepancy in the parameters between the open access Double Gyre code and paper [24]. We hope that this is the reason why we have some quantitative differences. If it is not mentioned, we do not

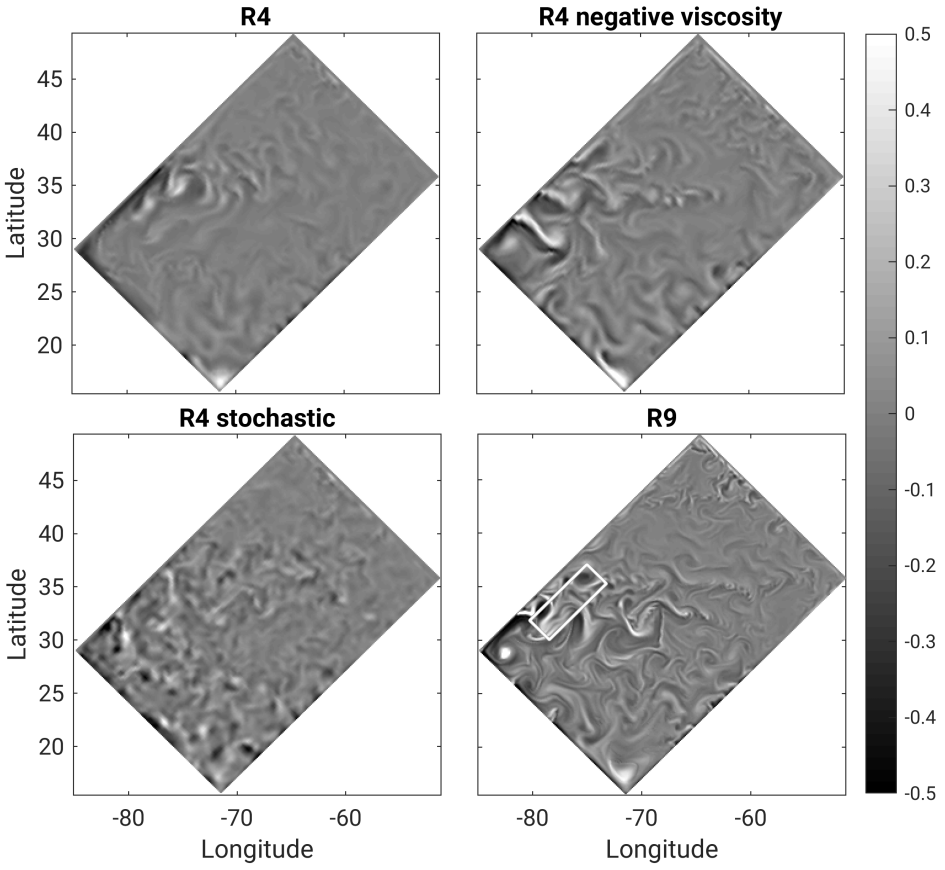

Fig. 1: Snapshot of surface relative vorticity in f (Coriolis parameter) units. 30 March after spin-up. R4 – eddy-permitting model, R9 – eddy-resolving model, R4 negative viscosity and R4 stochastic – eddy-permitting models with KEB parameterizations. Colorbar is saturated at ± 0.5. The white rectangle is explained in Fig. 10.

change the source code. The ocean model solves primitive equations (the vectors are in bold):

$$\frac{\mathrm{d}T}{\mathrm{d}t} = F_T, \qquad \frac{\mathrm{d}S}{\mathrm{d}t} = F_S \tag{1.1}$$

$$\frac{\partial \mathbf{U}_h}{\partial t} + \mathrm{adv}_h + \mathrm{cor}_h = -\frac{1}{\rho_0}\nabla_h p + \mathbf{F}_{\mathbf{U}_h} \tag{1.2}$$

$$\frac{\partial \eta}{\partial t} = -H\nabla_h \overline{\mathbf{U}}_h \tag{1.3}$$

$$\frac{\partial p}{\partial z} = -\rho g, \qquad \nabla \cdot \mathbf{U} = 0 \tag{1.4}$$

$$\rho = \rho_0(1 - a(T - T_0) + b(S - S_0)) \tag{1.5}$$

where T, S, $\mathbf{U}$, η, ρ, and p are the potential temperature, salinity, velocity, free surface height, density, and pressure, respectively; $\mathbf{U}_h$ is the horizontal part of the velocity, and $\overline{\mathbf{U}}_h$ is its vertical average. F_T, F_S, $\mathbf{F}_{\mathbf{U}_h}$ are the external forcings and physical parameterizations. We introduce a Lagrangian derivative $\mathrm{d}/\mathrm{d}t = \partial/\partial t + (\mathbf{U}\cdot\nabla)$, a nabla operator $\nabla = (\partial_x, \partial_y, \partial_z)$, and its horizontal part $\nabla_h = (\partial_x, \partial_y)$. Exact expressions for the advective and Coriolis terms adv_h and cor_h are given in [26]. We use TVD and energy-conserving scheme for scalars and momentum advection, respectively (see [26]). In our configuration the free surface equation (1.3) and the equation of state (1.5) are linear. The EOS parameters are as follows: $\rho_0 = 1026\,\mathrm{kg\,m^{-3}}$, $a = 2\cdot 10^{-4}\mathrm{K}^{-1}$, $b = 7.7\cdot 10^{-4}\mathrm{psu}^{-1}$, $T_0 = 10^{\circ}\,\mathrm{C}$, $S_0 = 35\mathrm{psu}$. The computational domain is a flat-bottomed rectangular box $L_x \times L_y \times L_z = 3180\,\mathrm{km} \times 2120\,\mathrm{km} \times 4\,\mathrm{km}$ in the β-plane approximation with free-slip and no heat flux, no salt flux spatial boundary conditions, and quadratic bottom drag. The basin is centered at

Tab. 1: Model experiments (R1, R4, R9) and their parameters. Unless otherwise mentioned, diffusivity/viscosity acts in horizontal direction.

	R1 non-eddy-resolving	R4 eddy-permitting	R9 eddy-resolving
$n_x \times n_y \times n_z$	$30 \times 20 \times 30$	$120 \times 80 \times 30$	$270 \times 180 \times 30$
mesh step	1°, 106 km	1/4°, 26.5 km	1/9°, 11.7 km
time step	120 min	30 min	800 sec
eddy diffusivity	isoneutral ∇_h^2, $10^3 \mathrm{m}^2 s^{-1}$	∇_h^4, $-10^{10} \mathrm{m}^4 s^{-1}$	∇_h^4, $-10^9 \mathrm{m}^4 s^{-1}$
eddy viscosity	∇_h^2, $10^5 \mathrm{m}^2 s^{-1}$	∇_h^4, $-5 \cdot 10^{11} \mathrm{m}^4 s^{-1}$	∇_h^4, $-5 \cdot 10^{10} \mathrm{m}^4 s^{-1}$

$\sim 30°$ N and rotated by 45° to the zonal direction in lat-lon coordinates (see Fig. 1). Note that the metric terms inherent to spherical geometry are excluded.

The free surface is stressed by zonal wind with maximum eastward speed at 36° N and maximum westward speed at 22° N. The following three surface buoyancy fluxes sustain a south-north decline of the surface temperature and salinity. The conductive heat flux from the atmosphere is given by $Q = \gamma\,(T_{\mathrm{atm}} - T_{\mathrm{SST}})$, T_{SST} and T_{atm} are the surface ocean temperature and atmosphere temperature, respectively, $\gamma = 40\ \mathrm{W\,m^{-2}\,K^{-1}}$. Also, solar radiation and fresh water fluxes are prescribed at the surface. The listed forcings vary with latitude and seasonally and are given in [24].

We consider models with three uniform spatial resolutions. The parameters are given in Table 1. R1 model is initialized at rest with vertical profiles of temperature and salinity uniformly applied to the whole basin [24]. We accomplish spin-up of R4 and R9 models, first running R1 model for 1000 years and then continuing the computations with R4 or R9 models for 120 years. The last 20 years are stored for analysis. The Rossby deformation radius for the resulting stratification varies from 40 km in the south to 5 km in the north [24]. The diffusion/viscosity coefficients for models R1 and R9 are taken from [24]. The viscosity in model R4 is almost the smallest possible. Further decreasing leads to wrong reproduction of the meridional eddy heat flux, as will be shown below.

2 Kinetic energy backscatter (KEB) parameterizations

2.1 Negative viscosity KEB

This parameterization supplements horizontal biharmonic momentum damping in the momentum equation (1.2) with additional negative viscosity term returning energy, as proposed in [12]:

$$\frac{\partial \mathbf{U}_h}{\partial t} = \cdots + \nu_4 \nabla_h^4 \mathbf{U}_h + \nabla_h \left(\nu_2 \nabla_h \mathbf{U}_h\right). \tag{2.1}$$

Here ∇_h is assumed to act on the vector componentwise. When $\nu_4 < 0$, the grid-scale numerical noise is effectively dissipated. The viscosity $\nu_2 \leqslant 0$ must be negative to return the energy. The choice of negative viscosity term for KEB is natural, since it is one of the simplest linear operators with a characteristic length scale larger than that of the biharmonic operator. Moreover, it is shown by R. Kraichnan in [23] that subgrid 2D turbulence produces a tendency represented by the Laplace operator in the middle and large scales with a negative viscosity coefficient. To take into consideration spatial non-homogeneity of the eddy field and weak dynamics near the bottom, we follow works [13, 15, 38] and introduce dependence on the coordinates $\nu_2(x, y, z, t) \leqslant 0$, ν_2 is found based on the 'energetically consistent' property: the joint energy flux to subgrid scales corresponding to the negative viscosity and biharmonic terms must be zero. This property is consistent with the idea of inverse energy cascade: the energy shall not pass to subgrid scales. The energy fluxes to subgrid scales related to the biharmonic and negative viscosity terms are expressed in Galilean invariant

form following [38]:

$$\dot{E}_{\text{diss}} = \nu_4 \nabla_h \mathbf{U}_h \cdot \nabla_h \left(\nabla_h^2 \mathbf{U}_h \right) \tag{2.2}$$

$$\dot{E}_{\text{back}} = \nu_2 \nabla_h \mathbf{U}_h \cdot \nabla_h \mathbf{U}_h. \tag{2.3}$$

The signs of the fluxes are as follows: $\int \dot{E}_{\text{diss}} \mathrm{d}x\mathrm{d}y\mathrm{d}z > 0$, $\int \dot{E}_{\text{back}} \mathrm{d}x\mathrm{d}y\mathrm{d}z \leqslant 0$. Local equalization of these fluxes $\dot{E}_{\text{diss}}(x, y, z, t) + \dot{E}_{\text{back}}(x, y, z, t) = 0$ leads to an ill-posed problem for finding ν_2 if $|\nabla_h \mathbf{U}_h| = 0$. To overcome it, papers [13] and [38] introduced an equation for subgrid energy ($e \equiv e(x, y, z, t)$), which is produced by dissipation ($\dot{E}_{\text{diss}}$) and lost to the resolved scales ($\dot{E}_{\text{back}}$):

$$\frac{\mathrm{d}e}{\mathrm{d}t} = c_{\text{diss}} \dot{E}_{\text{diss}} + \dot{E}_{\text{back}} + \nu_e \nabla_h^2 e. \tag{2.4}$$

Here $\mathrm{d}/\mathrm{d}t$ is the Lagrangian derivative (advection), which is implemented in the code with the simplest upwind scheme [26], $\nu_e = 1000 \mathrm{m}^2 \mathrm{s}^{-1}$ is equal to the diffusivity of eddies in model R1. Contrary to [38], we apply the Lagrangian derivative instead of a partial derivative, which seems to be more physical and was originally proposed for the subgrid energy equation in [10]. As in [15], $c_{\text{diss}} \in (0, 1)$ allows one to reduce the backscatter power. We found $c_{\text{diss}} = 0.8$ to be satisfactory. Larger values produce overestimated strong vortices and a strong meridional eddy heat flux near the surface at the WBC separation latitude. The subgrid energy e defines the negative viscosity coefficient:

$$\nu_2 = -c_{\text{back}} \Delta x \sqrt{\max(e, 0)} \tag{2.5}$$

where Δx is the grid spacing and $c_{\text{back}} = 0.4\sqrt{2}$, as in [13]. Despite the fact that $\int \dot{E}_{\text{diss}} \mathrm{d}x\mathrm{d}y\mathrm{d}z > 0$, local values of $\dot{E}_{\text{diss}}$ may be negative, thus producing negative values of e. Introducing of max-function turns off KEB at these points. Neumann boundary conditions for the terms $\nabla_h(\nu_2 \nabla_h \mathbf{U}_h)$ in (2.1) and $\nu_e \nabla_h^2 e$ in (2.4) are applied: $(\nabla_h \mathbf{U}_h) \cdot \mathbf{n} = 0$ and $(\nabla_h e) \cdot \mathbf{n} = 0$, $\mathbf{n}$ is the normal vector to the horizontal boundary. As in [13], we report weak sensitivity of the results on the model for e used. Our understanding is that an additional equation for subgrid energy is required only to make the problem for determining ν_2 well-posed. In the next section it will be shown that the stochastic KEB can be tuned without an additional equation for subgrid energy.

2.2 Stochastic KEB

Let us construct a quasi-barotropic (quasi-2D) stochastic streamfunction as proposed in [4]:

$$\psi(x, y, z, t^n) = \varphi(x, y, t^n) \cdot A(x, y, z, t^n) \tag{2.6}$$

where $\varphi(x, y, t^n)$ is a discrete random field, i.e., φ is independent $N(0, 1)$ variables at each mesh point and time layer t^n (discrete-space-time white noise) with zeros at the boundary, A is the amplitude controlling the energy input. The streamfunction modifies the momentum equation (1.2) as follows:

$$\frac{\partial \mathbf{U}_h}{\partial t} = \cdots + \alpha \nabla_h^\perp S^n(\psi) \tag{2.7}$$

where $\nabla_h^\perp = (-\partial_y, \partial_x)$, α will be defined later. The function $S^n(\cdot)$ introduces n applications of a spatial discrete filter:

$$S(\psi) = \psi + \frac{(\Delta x)^2}{8} \nabla_h^2 \psi. \tag{2.8}$$

This filter is based on the Laplace operator already contained in the model and nullifies the checkerboard grid noise ($(-1)^{i+j}$, i and j are indices along the x- and y- directions) if a second order approximation is used. Zero Dirichlet boundary conditions are applied. The physical reasoning for stochastic parameterization with lateral white noise is again taken from [23], where subgrid turbulence was shown to produce stochastic forcing in small resolved scales. In contrast to [19], we generate random streamfunction, instead of random Reynolds stress components. Streamfunction approach gives analogous wavenumber spectrum, but does not

require removing divergence of the resulting forces in momentum equation [6]. According to [19], the filter $S^n(\cdot)$ defines the correlation radius of the resulting parameterization and can be considered as a correction of a sharp wavenumber spectrum near the grid scale to account for numerical effects of non-spectral advection schemes. We use $n = 6$, which gives a correlation radius of several mesh points.

Contrary to the negative viscosity KEB, local equalization of the energy fluxes $\dot{E}_{\text{diss}}$ and $\dot{E}_{\text{back}}$ is possible without an additional equation for subgrid energy. According to [1], energy generation by the white noise process is proportional to the squared amplitude ($\dot{E}_{\text{back}} \sim -A^2$) and, hence, we choose:

$$A\left(x, y, z, t^n\right) = \sqrt{\max\left(\dot{E}_{\text{diss}}, 0\right)}. \tag{2.9}$$

Finally, the energy generation and dissipation fluxes integrated over the domain should be equal. Again, using [1] we compute the energy generation for white noise and obtain a relation for finding the only free parameter α:

$$\frac{\alpha^2 \Delta t}{2} \int \left\langle \left|\nabla_h^{\perp} S^n(\psi)\right|^2 \right\rangle \mathrm{d}x\mathrm{d}y\mathrm{d}z = c_{\text{diss}} \int \dot{E}_{\text{diss}} \mathrm{d}x\mathrm{d}y\mathrm{d}z. \tag{2.10}$$

Here Δt is the time step, and the angle brackets $\langle\cdot\rangle$ denote averaging over realizations of the random field φ. The left-hand side of the above equation can be estimated analytically taking into consideration knowledge of the wavenumber spectra [4], but still with simplifications. Our novelty is to drop averaging over an ensemble:

$$\int \left\langle \left|\nabla_h^{\perp} S^n(\psi)\right|^2 \right\rangle \mathrm{d}x\mathrm{d}y\mathrm{d}z \approx \int \left|\nabla_h^{\perp} S^n(\psi)\right|^2 \mathrm{d}x\mathrm{d}y\mathrm{d}z \tag{2.11}$$

where the right-hand side is computed directly for the current realization of φ. This method is based on the following facts: (1) the ensemble-mean of RHS equals LHS and (2) the standard deviation of RHS is 7% of its mean value. Optimal value of c_{diss} is 1, in contrast to 0.8 in negative viscosity KEB. It can be explained by the fact that stochastic KEB excites inertial waves which are extensively dissipated by the numerical filter applied to the free surface equation (see [26]).

3 Results

The model in Double Gyre setting simulates the western boundary current (WBC) similar to Gulfstream or Kuroshio. At some latitude, the WBC separates from the boundary forming, in the zonal direction, an offshore extension which divides the north and south gyres (see Fig. 1). The separation latitude is strongly dependent on the resolution, and it moves to the south as the mesoscale and submesoscale eddies become resolved [24]. The WBC separation point and its extension strength are strongly associated with the sea surface temperature (SST) and the sea surface height (SSH), since their isolines pass along the jet current.

Below, we consider 4 models: an eddy-permitting model R4, an eddy-resolving model R9, and R4 with two KEB parameterizations: negative viscosity and stochastic ones. They are spun up as described in Section 1.

3.1 Eddy kinetic energy

Strength of the eddy activity can be attributed to the eddy kinetic energy (EKE) level ($\langle \mathbf{u}'^2 \rangle/2$, where $\mathbf{u}'$ is the deviation from the time mean $\langle \mathbf{u} \rangle$ over the last 20 years). Applying the KEB parameterizations allows one to increase the lateral mean EKE of coarse models approximately up to the level of model R9 at all depths (see Fig. 2). In contrast to work [15], where coarse models with KEB work fine over the whole depth, we report overestimated EKE after KEB applying at depth more than 200 m. Spatial distribution of surface EKE is given in Fig. 3 in colour. Both KEB parameterizations lead to shift of surface EKE maximum southward, which is consistent with reference model (R9) prediction. However, we point out that the surface EKE in models R4 with KEBs is elongated along the boundary, contrary to elongation in the zonal direction in model R9. It means that long jet extension cannot be simulated at a coarse grid even with these KEB parameterizations.

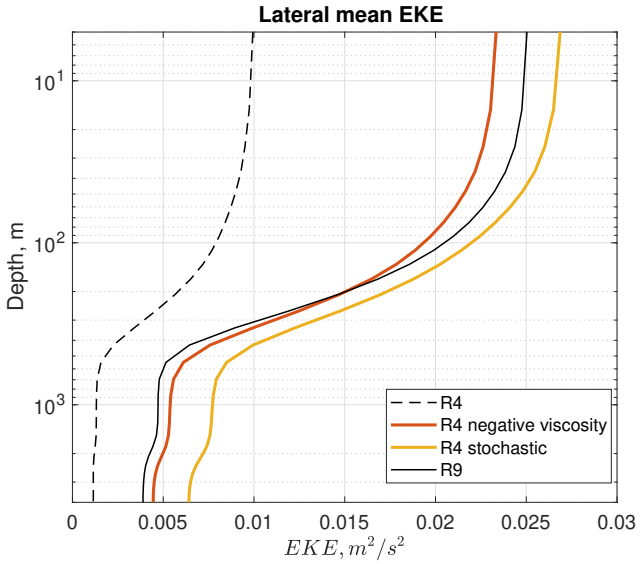

Fig. 2: 20-year mean eddy kinetic energy (EKE) averaged laterally as a function of depth, m^2/s^2. Comparison of eddy-permitting (R4, R4+KEBs) and eddy-resolving (R9) models.

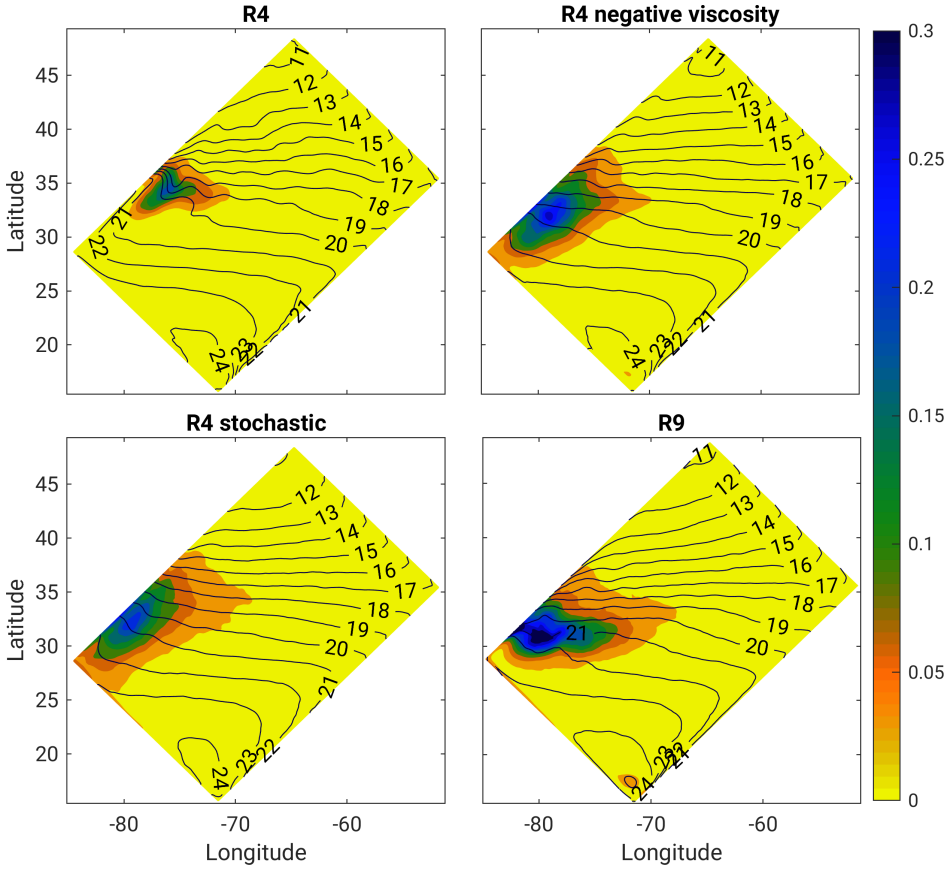

Fig. 3: In colour: 20-year mean surface eddy kinetic energy (EKE), m^2/s^2. The colorbar is saturated at 0.3. In contours: 20-year mean sea surface temperature (SST), ° C. Comparison of eddy-permitting (R4, R4+KEBs) and eddy-resolving (R9) models.

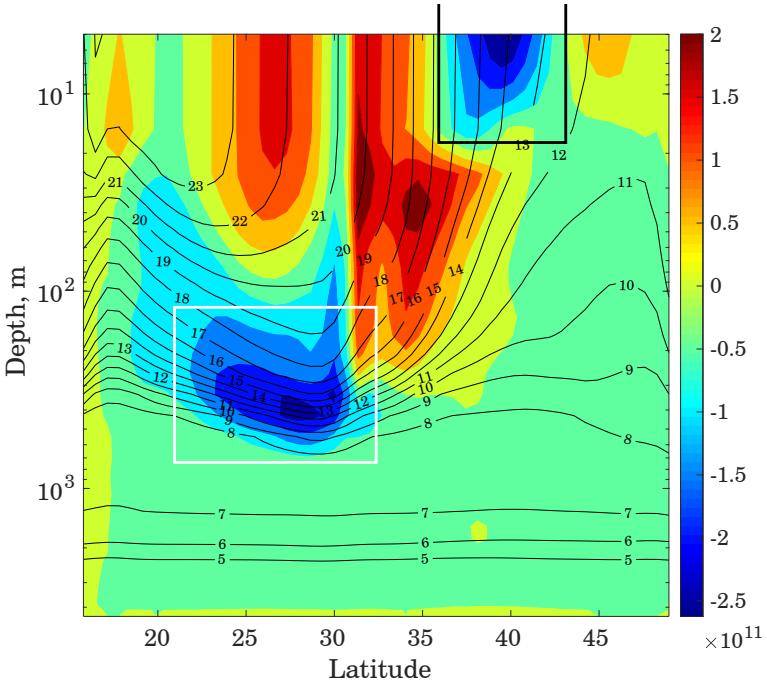

Fig. 4: In colour: 20-year mean eddy meridional heat transport integrated zonally, W/m. In contours: 20-year mean zonally averaged potential temperature. Results for R9 model. Black rectangle shows strong along-gradient flux. White rectangle shows strong southward anti-gradient flux.

3.2 Eddy heat flux

One of the most important characteristics of the eddy activity is the transport of scalars. Under the prescribed surface heat fluxes, ocean flows produce meridional heat transport (MHT) towards north: $Q = \rho_0 C_p TV$, where $C_p \approx 3992 \mathrm{JK}^{-1}\mathrm{kg}^{-1}$ is the heat capacity, and V is the meridional velocity; its dimension is $[Q] = \mathrm{W/m}^2$. Note that we neglect the diffusion heat transport, since its action is minimized with the use of a biharmonic operator. The MHT consists of two parts: mean-flow meridional heat transport (MMHT),

$$\rho_0 C_p \langle T \rangle \langle V \rangle \tag{3.1}$$

where the angle brackets stand for time-averaging over the last 20 years, and the rest – eddy meridional heat transport (EMHT),

$$\rho_0 C_p (\langle TV \rangle - \langle T \rangle \langle V \rangle). \tag{3.2}$$

In case of nonzero integral flow across zonal cross-section, MHT can depend on the units of potential temperature, $^\circ$C or K. So, we present here independent EMHT only. The EMHT strongly varies with resolution: it is almost zero for model R1, but high resolution simulations have a significant EMHT, of the order of the MMHT and in opposite direction (see [24] for details).

As far as the northern gyre is colder than the southern one, we expect eddy heat flux to be directed northward, i.e., in the direction opposite to the surface temperature gradient. As follows from Fig. 4, where the distribution of the EMHT in depth for model R9 is given, EMHT is northward only in the surface layer 200 m deep. Exception to the rule is the surface region 37°–42° N, where strong along-gradient eddy heat flux occur, see black rectangle in Fig. 4. The most significant EMHT (note the logarithmic depth-scale) corresponds to a region 200 m–500 m in depth and 23°–30° N, which is shown by the white rectangle in Fig. 4. The heat in this region fluxes southward, which is consistent with the northward gradient of potential temperature at this depth. This flux determines a sign of depth-integrated EMHT in southern gyre (see Fig. 6). Both KEB parameterizations amplify this negative flux in model R4 (see Fig. 5), and break the wrong negative heat flux

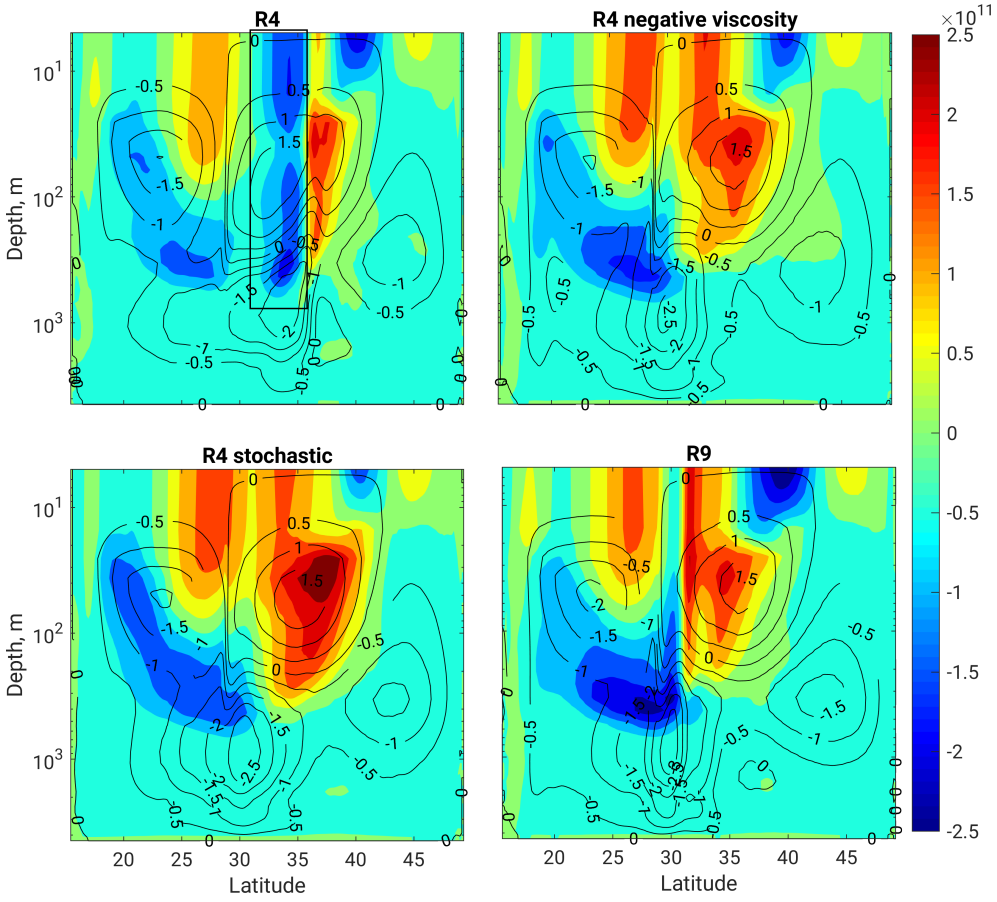

Fig. 5: In colour: 20-year mean eddy meridional heat transport integrated zonally, W/m. In contours: 20-year mean meridional overturning streamfunction Ψ_{MOC} in Sverdrups. Comparison of eddy-permitting (R4, R4+KEBs) and eddy-resolving (R9) models. Black rectangle shows wrong southward heat flux.

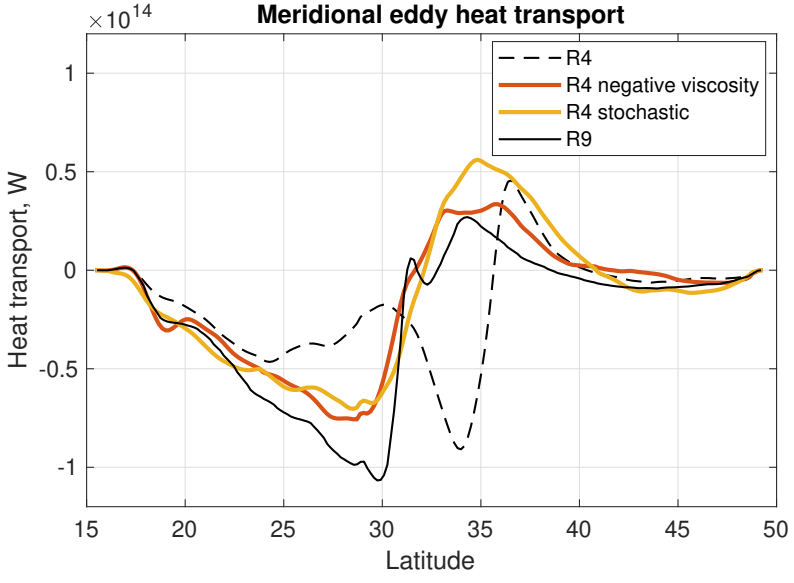

Fig. 6: 20-year mean meridional eddy heat transport integrated zonally and in depth, W. Comparison of eddy-permitting (R4, R4+KEBs) and eddy-resolving (R9) models.

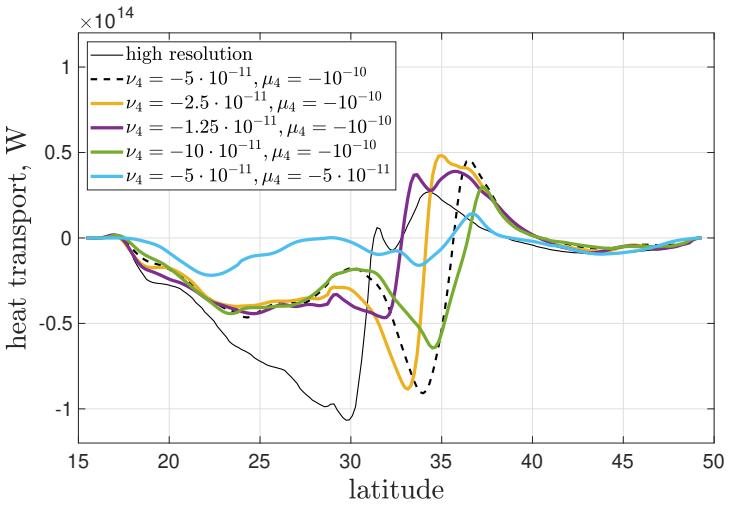

Fig. 7: 20-year mean meridional eddy heat transport integrated zonally and in depth, W. Solid black line corresponds to R9 model, dashed black line to R4. Colour lines stand for R4 model with deviating viscosity (ν_4) and diffusivity (μ_4).

in the region 32°–35° N, see black rectangle. Both KEBs allow us to shift latitude of maximum negative depth-integrated heat flux in south direction, although its maximum negative value is underestimated (see Fig. 6). Also, models with KEBs overestimate positive depth-integrated heat flux north of 30° N (see Fig. 6). The effect of shifting the latitude of maximum negative EMHT cannot be achieved by adjusting viscosity (ν_4) or diffusion (μ_4) coefficients (see Fig. 7).

3.3 Mean fields

The meridional overturning circulation (MOC) is shown by contours in Figure 5. The MOC is described by the following streamfunction: $\Psi_{MOC}(y',\ z) = \int_{-H}^{-z} \langle V(x', y', z', t)\rangle \mathrm{d}x'\mathrm{d}z'$, where x' and y' are the coordinates along longitude and latitude, respectively, $z \in (-H, 0)$ is the depth, the angle brackets is time averaging over the last 20 years and V is the meridional velocity. The circulation in all models consists of 4 cells, and the largest one is at the bottom (note logarithmic depth-scale). This cell is shifted northward in model R4 as compared to R9. Both KEB parameterizations restore the correct position of the bottom cell at about 30° N. The upper northern cell acquires correct shape as a result of applying the KEBs. Stochastic KEB reproduces northern bottom cell better than negative viscosity one (see −1.5 isoline in Fig. 5).

Improvements in eddy activity and mean circulation have positive impact on mean surface fields. Figure 3 shows the 20-year mean SST in contours for 4 models. The major discrepancy between models R4 and R9 is in isotherms 21 and 22. Applying the KEB straightens these isotherms, which leads to a significant fall of the errors in the mean SST. See Table 2 for errors in mean fields (SST, SSH, SSS). Spatial distribution of deviations of SST and SSH with respect to model R9 is shown in Figs. 8 and 9, respectively. As a result of both KEBs applying, errors fall near jet separation point, while negative viscosity KEB introduces additional errors at the north.

3.4 Time variability

We study the time variability of the models by computing the time power density of the surface EKE (see Fig. 10). The power density is averaged over a white rectangle shown in Fig. 1 to reduce its oscillations and to exclude its strong dependence on the WBC separation point. The spectra consist of two power-law intervals (ν^{-4}, ν^{-2}) and a long-period tail. We do not give the physical reasoning for the power laws, but guess that

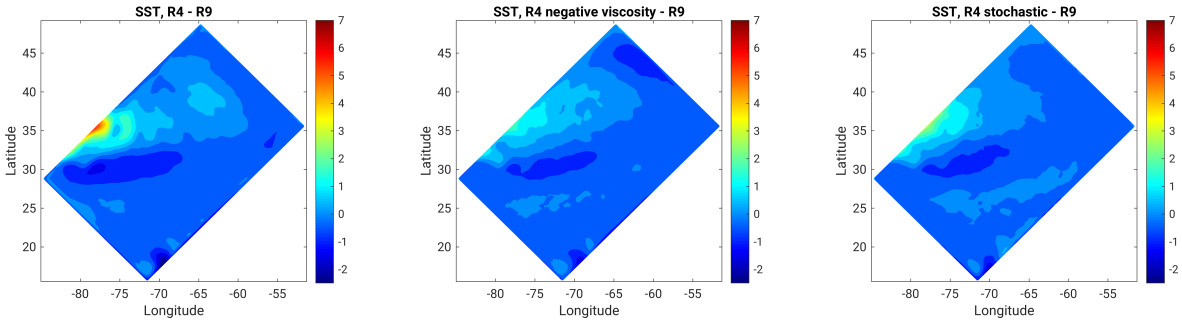

Fig. 8: 20-year mean difference in SST (Sea surface temperature) between eddy-permitting (R4, R4+KEBs) models and eddy-resolving R9 reference, ° C.

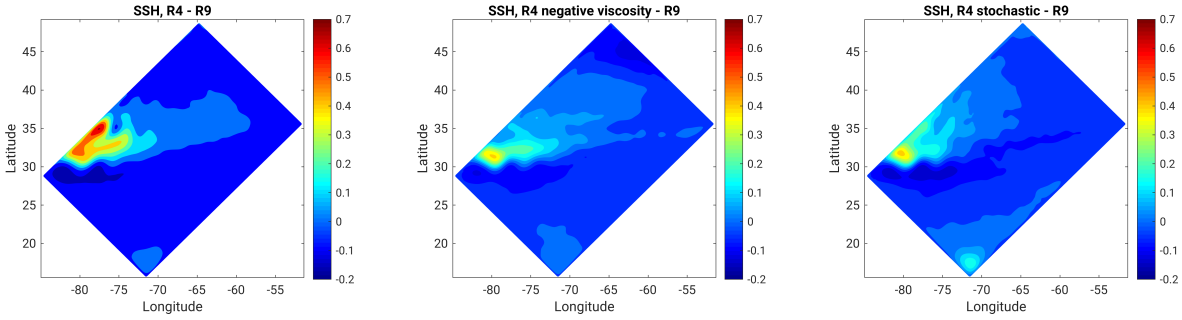

Fig. 9: 20-year mean difference in SSH (Sea surface height) between eddy-permitting (R4, R4+KEBs) models and eddy-resolving R9 reference, m.

Tab. 2: Norms of errors in 20-year mean SST, SSH, SSS (sea surface temperature / height / salinity) between coarse (R4, R4 + KEBs) models and R9 reference. The following two norms for any $\varphi(x, y)$ are separated by the semicolon: $\max(|\varphi_{R4} - \varphi_{R9}|)$; $\mathrm{mean}(|\varphi_{R4} - \varphi_{R9}|)$.

	R4	R4 negative viscosity	R4 stochastic
SST, ° C	7.0; 0.4	3.1; 0.3	4.3; 0.27
SSH, m	0.68; 0.062	0.38; 0.039	0.40; 0.040
SSS, psu	0.54; 0.108	0.33; 0.098	0.52; 0.070

the change in the slope at a 5-day frequency is related to the absence of mesoscale dynamics on smaller time scales. Both power-law intervals are underestimated in model R4. The KEB parameterizations allow one to increase the power density in the middle interval ν^{-2} up to the level of model R9. The negative viscosity KEB also improves the power density in the short-period interval ν^{-4}. The stochastic KEB gives discrepancy with model R9 in the short-period tail and has a singularity near 1-day oscillation. We guess that the white-noise parameterization excites inertial waves which have a similar period. Earlier it was not reported anywhere that KEB with the white-noise stochastic process excites inertial waves, possibly since most works consider quasi-geostrophic equations (e.g., [12, 19]), where inertial oscillations are filtered out. We have tried a simple modification of the stochastic KEB, including a temporal correlation with a lag of 1 day to force only the middle-period interval. Correlated noise was generated using an autoregressive model of order 1 (AR-1), as [4] suggests. The time-correlated stochastic KEB does not excite inertial oscillations (not shown), but it has one moderate drawback: there is no more exact formula for the energy generation like (2.10), and it introduces one free parameter (α) to be tuned by hand.

Finally, let us consider snapshots of relative vorticity (see Fig. 1). The R4 and R9 solutions are highly different in the number of turbulent eddies and filaments. Both KEB parameterizations induce eddy activity in model R4, but in different way. The stochastic KEB solution looks like ‘synthetic’ turbulence which consists of turbulent eddies without filaments, and it is similar in the shape of its eddies to the stochastic KEB tendency

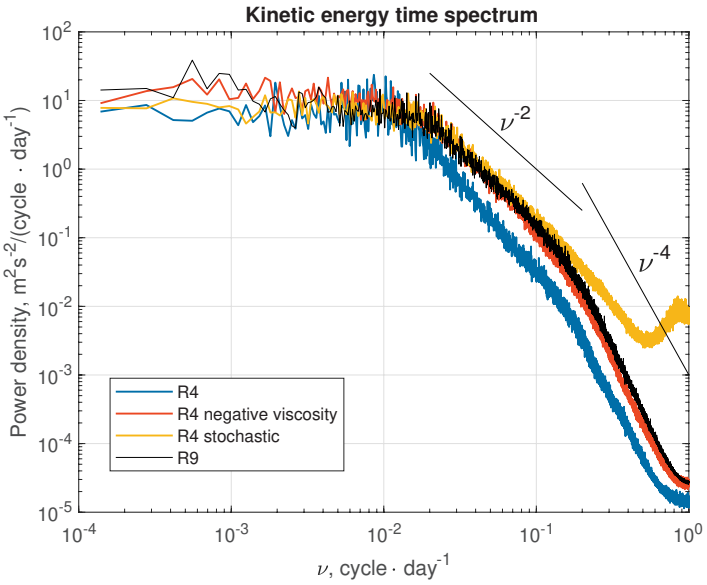

Fig. 10: Time power density of surface EKE. Density is averaged over a white rectangle shown in Fig. 1. Time series correspond to the last 20 years.

itself. The amount of undesirable noise in the solution can be reduced if the time-correlated stochastic process is used (not shown). The negative viscosity KEB, on the contrary, amplifies the existing filaments and large eddies, but the solution suffers from the absence of small-scale features.

4 Conclusions

In this work, we have demonstrated that simple kinetic energy backscatter (KEB) parameterizations accounting for a badly resolved barotropic inverse energy cascade are able to improve general ocean circulation models with an eddy-permitting resolution. The novelty of this work is the comparison of two KEBs, stochastic and negative viscosity, in the primitive-equations ocean model. Both KEBs give similar improvements in the mean characteristics. Specifically, the mesoscale eddies are amplified and, consequently, eddy kinetic energy (EKE) rises. As a result, the eddy meridional heat transport near the surface and in a moderately deep ocean was restored. Large errors in the sea surface temperature and height were reduced in the region of jet separation. Also, the bottom cell of the meridional overturning circulation (MOC) was shifted southward, as in the high resolution model. A moderate difference concerns the bottom northern MOC cell, which is better reproduced with the stochastic KEB. It has been shown that the KEBs effectively improve the time power spectra of EKE, but a white-noise process can lead to an undesirable generation of inertial waves, which can be overcome by introducing a time-correlated stochastic process. The major difference between the KEBs is in the solution type. The stochastic KEB seems to introduce too much small eddies without filaments, but the negative viscosity one amplifies the existing filament-eddy field. Future work will be devoted to studying more realistic ocean configurations with varying ocean depth and spherical geometry.

Acknowledgment: Author would like to thank A. V. Glazunov and N. G. Yakovlev for helpful comments and discussion.

Funding: Analysis of the results and their interpretation were carried out with the financial support of the Russian Foundation for Basic Research (projects 19-35-90023, 18-05-60184). The development of computing

technologies was carried out with the financial support of the Russian Ministry of Education and Science (agreement No. 075-15-2019-1624).

References

[1] K. Alvelius, Random forcing of three-dimensional homogeneous turbulence. *Physics of Fluids* **11** (1999), No. 7, 1880–1889.
[2] J. Bardina, J. Ferziger, and W. Reynolds, Improved subgrid-scale models for large-eddy simulation. In: *13th Fluid and Plasma Dynamics Conference*, 1980, p. 1357.
[3] P. Berloff, Dynamically consistent parameterization of mesoscale eddies. Part III: Deterministic approach. *Ocean Modelling* **127** (2018), 1–15.
[4] J. Berner, G. Shutts, M. Leutbecher, and T. Palmer, A spectral stochastic kinetic energy backscatter scheme and its impact on flow-dependent predictability in the ECMWF ensemble prediction system. *J. Atmosph. Sci.* **66** (2009), No. 3, 603–626.
[5] F. Bouchet, Parameterization of two-dimensional turbulence using an anisotropic maximum entropy production principle (2003). arXiv:cond-mat/0305205
[6] D. Carati, S. Ghosal and P. Moin, On the representation of backscatter in dynamic localization models. *Phys. Fluids* **7** (1995), No. 3, 606–616.
[7] J. Chasnov, Simulation of the Kolmogorov inertial subrange using an improved subgrid model. *Phys. Fluids A: Fluid Dynamics* **3** (1991), No. 1, 188–200.
[8] S. Dwivedi, C. Franzke, and F. Lunkeit, Energetically consistent scale-adaptive stochastic and deterministic energy backscatter schemes for an atmospheric model. *Q. J. Royal Meteorol. Soc.* (2019), 1–11.
[9] V. Dymnikov and P. Perezhogin, Systems of Hydrodynamic Type that Approximate Two-Dimensional Ideal Fluid Equations. *Izvestiya, Atmospheric and Oceanic Physics* **54** (2018), No. 3, 232–241.
[10] C. Eden and R. Greatbatch, Towards a mesoscale eddy closure. *Ocean Modelling* **20** (2008), No. 3, 223–239.
[11] J. Frederiksen and A. Davies, Eddy viscosity and stochastic backscatter parameterizations on the sphere for atmospheric circulation models. *J. Atmos. Sci.* **54** (1997), No. 20, 2475–2492.
[12] M. Jansen and I. Held, Parameterizing subgrid-scale eddy effects using energetically consistent backscatter. *Ocean Modelling* **80** (2014), 36–48.
[13] M. Jansen, I. Held, A. Adcroft, and R. Hallberg, Energy budget-based backscatter in an eddy permitting primitive equation model. *Ocean Modelling* **94** (2015), 15–26.
[14] M. Jansen, A. Adcroft, S. Khani, and H. Kong, Toward an energetically consistent, resolution aware parameterization of ocean mesoscale eddies. *J. Advances in Modeling Earth Systems* **11** (2019), No. 8, 2844–2860.
[15] S. Juricke, S. Danilov, A. Kutsenko, and M. Oliver, Ocean kinetic energy backscatter parametrizations on unstructured grids: Impact on mesoscale turbulence in a channel. *Ocean Modelling* **138** (2019), 51–67.
[16] S. Juricke, S. Danilov, N. Koldunov, M. Oliver, and D. Sidorenko, Ocean kinetic energy backscatter parametrization on unstructured grids: Impact on global eddy-permitting simulations. *J. Advances in Modeling Earth Systems* **12** (2020), e2019MS001855.
[17] R. Haarsma and Coauthors, High Resolution Model Intercomparison Project (HighResMIP v1.0) for CMIP6. *Geosci. Model Dev.* **9** (2016), No. 11, 4185—4208.
[18] M. Germano, U. Piomelli, P. Moin, and W. Cabot, A dynamic subgrid-scale eddy viscosity model. *Physics of Fluids A: Fluid Dynamics* **3** (1991), No. 7, 1760–1765.
[19] I. Grooms, Y. Lee, and A. Majda, Numerical schemes for stochastic backscatter in the inverse cascade of quasigeostrophic turbulence. *Multiscale Modeling & Simulation* **13** (2015), No. 3, 1001–1021.
[20] I. Grooms and A. Majda, Stochastic superparameterization in quasigeostrophic turbulence. *J. Comput. Physics* **271** (2014), 78–98.
[21] J. Kent, C. Jablonowski, J. Thuburn, and N. Wood, An energy-conserving restoration scheme for the shallow-water equations. *Q. J. Royal Meteorol. Soc.* **142** (2016), No. 695, 1100–1110.
[22] R. Kraichnan, Inertial ranges in two-dimensional turbulence. *Physics of Fluids* **10** (1967), No. 7, 1417–1423.
[23] R. Kraichnan, Eddy viscosity in two and three dimensions. *J. Atmos. Sci.* **33** (1976), No. 8, 1521–1536.
[24] M. Lévy, P. Klein, A. Tréguier, D. Iovino, G. Madec, S. Masson, and K. Takahashi, Modifications of gyre circulation by sub-mesoscale physics. *Ocean Model.* **34** (2010), No. 1–2, 1–15.
[25] G. Madec et al., Ocean general circulation model reference manual. *Note du Pôle de modélisation* (1997).
[26] G. Madec et al., NEMO ocean engine. *Institut Pierre-Simon Laplace* (2015).
[27] P. Mana and L. Zanna, Toward a stochastic parameterization of ocean mesoscale eddies. *Ocean Modelling* **79** (2014), 1–20.
[28] R. Maulik and O. San, A stable and scale-aware dynamic modeling framework for subgrid-scale parameterizations of two-dimensional turbulence. *Computers & Fluids* **158** (2017), 11–38.

[29] R. Maulik, O. San, A. Rasheed and P. Vedula, Subgrid modelling for two-dimensional turbulence using neural networks. *J. Fluid Mechanics* **858** (2019), 122–144.
[30] P. Perezhogin, 2D turbulence closures for the barotropic jet instability simulation. *Russ. J. Numer. Anal. Math. Modelling* **35** (2020), No. 1, 21–35.
[31] P. Perezhogin, A. Glazunov, and A. Gritsun, Stochastic and deterministic kinetic energy backscatter parameterizations for simulation of the two-dimensional turbulence. *Russ. J. Numer. Anal. Math. Modelling* **34** (2019), No. 4, 197–213.
[32] P. Perezhogin and V. Dymnikov, Modeling of quasi-equilibrium states of a two-dimensional ideal fluid. *Doklady Physics* **62** (2017), No. 5, 248–252.
[33] P. Perezhogin, A. Glazunov, E. Mortikov, and V. Dymnikov, Comparison of numerical advection schemes in two-dimensional turbulence simulation. *Russ. J. Numer. Anal. Math. Modelling* **32** (2017), No. 1, 47–60.
[34] P. Perezhogin and V. Dymnikov, Equilibrium states of finite-dimensional approximations of a two-dimensional incompressible inviscid fluid. *Nonlinear Dynamics* **13** (2017), No. 1, 55–79 (In Russian).
[35] P. Sagaut, *Large Eddy Simulation for Incompressible Flows: an Introduction*. Springer, Heidelberg, 2005.
[36] J. Thuburn, J. Kent, and N. Wood, Cascades, backscatter and conservation in numerical models of two-dimensional turbulence. *Q. J. Royal Meteorol. Soc.* **140** (2014), No. 679, 626–638.
[37] L. Zanna, P. Mana, J. Anstey, T. David, and T. Bolton, Scale-aware deterministic and stochastic parametrizations of eddy-mean flow interaction, *Ocean Modelling*, **111** (2017), 66–80.
[38] P. Zurita-Gotor, I. Held, and M. Jansen, Kinetic energy-conserving hyperdiffusion can improve low resolution atmospheric models. *J. Adv. Modeling Earth Sys.* **7** (2015), No. 3, 1117–1135.